Low Symmetrical Phthalocyanine Analogues Substituted with Three Crown Ether Voids and Their Cation-Induced Supermolecules

Nagao Kobayashi,* Mika Togashi,† Tetsuo Osa,† Kazuyuki Ishii,‡ Seigo Yamauchi,‡ and Hiroaki Hino§

Contribution from the Department of Chemistry, Pharmaceutical Institute, Institute for Chemical Reaction Science, Tohoku University, Sendai 980-77, Japan, and School of Business Administration, Ishinomaki Senshu University, Ishinomaki 986, Japan

Received March 21, 1995. Revised Manuscript Received September 15, 1995[⊗]

Abstract: Unsymmetrical phthalocyanine analogues with three 15-crown-5 ether voids at the 3,4-positions (MtNIL, MtBZ, MtNAP) (Mt = Zn, Cu) have been synthesized and characterized. Their dimerization is induced by addition of some cations, particularly Rb^{2+} and K^+. Cofacial dimer formation in the presence of these cations proceeds in a two-step three-stage process, as indicated by absorption and emission spectroscopy. These cofacial species have a highly specific C_{2v} eclipsed configuration providing well-defined dimeric species for spectroscopic analysis. The ESR spectra of the cation-induced dimeric copper derivatives show axial symmetry and may be analyzed in terms of interplanar separation of 4.2 Å. CuNAP alone forms a cofacial dimer even in the presence of Na^+ or Cs^+, and the estimated interplanar distances are 4.1−4.2 Å without depending on the size of cations. The ^{1}H NMR spectra of zinc dimers are consistent with a cofacial configuration. Magnetic circular dichroism (MCD) spectra of C_{2v} type monomers can be interpreted as the superimposition of Faraday *B*-terms. Upper excited state (Soret, S_2) emission is observed for all zinc mononuclear species, and the quantum yield of S_1 emission is smaller than that of zinc phthalocyanine containing four crown units (ZnCRPc), suggesting that the lowering of molecular symmetry produces a decrease in quantum yield. Fluorescence decay of S_1 and S_2 emissions can be analyzed by mono- and biexponential fits, respectively. The zero field splitting (zfs) parameters, *D*, of the excited triplet (T_1) states of the monomers estimated from time-resolved EPR (TREPR) technique decrease in the order ZnNIL, ZnBZ, and ZnNAP, qualitatively indicating delocalization of excited π-electrons over additionally fused benzo and naphtho rings. A remarkable decrease in *D* value on dimerization is interpreted as an indication of delocalization of π-electrons over two macrocycles. Molecular orbital (MO) calculations within the framework of the Pariser−Parr−Pople (PPP) approximation succeed to reproduce the splitting, intensity, and the relative position of the Q absorption band of unsymmetrical monomers.

Introduction

There has been considerable interest in the properties of the crown ether substituted phthalocyanines (Pcs)[1] and porphyrins.[2] One of the most important differences between these phthalocyanines and porphyrins appears when they form cation-induced cofacial dimers; the former exhibit eclipsed configurations, while the latter dimers are always staggered because of their structural limitation. Accordingly, it may not be particularly interesting to prepare porphyrins containing three crown ether units. Phthalocyanines with three crown ether units are, on the other hand, more attractive since aromatic compounds of varying size can be fused to the fourth position. That is, it may be possible to realize an eclipsed configuration of C_{2v} type phthalocyanine analogues. The properties of mononuclear C_{2v} type phthalocyanine analogues *per se* have scarcely been elucidated, although they seem to be important in fields, for example, using lasers such as photodynamic cancer therapy and optical discs. Accordingly, if in addition, we can show the possibility of cofacial dimer formation of such low symmetrical phthalocyanine analogues, it may further invoke the attention of many researchers. Also, such research seems important to understand the nature of phthalocyanines themselves. From such respect, we report here the synthesis and solution properties of mono-substituted C_{2v} type phthalocyanines with three 15-crown-5 ether voids (Figure 1). As shown below, spectroscopic properties of these lower symmetrical Pc derivatives are often quite different from those of Pcs with D_{4h} symmetry, but their cation-induced cofacial dimer formation was confirmed by several types of spectroscopy. The results are compared with those of four crown ether-linked phthalocyanine (MtCRPc) systems.[1]

† Pharmaceutical Institute.
‡ Institute for Chemical Reaction Science.
§ School of Business Administration.
⊗ Abstract published in *Advance ACS Abstracts,* January 15, 1996.

(1) Some representative ones: (a) Kobayashi, N.; Nishiyama, Y. *J. Chem. Soc., Chem. Commun.* **1986**, 1462. (b) Koray, A. R.; Ahsen, V.; Bekaroglu, O. *J. Chem. Soc., Chem. Commun.* **1986**, 932. (c) Sielcken, O. E.; Van de Kuil, L. A. Drenth, W.; Nolte, R. J. M. *J. Chem. Soc., Chem. Commun.* **1986**, 1232. (d) Sirlin, C.; Bosio, L.; Simon, J.; Ahsen, V.; Yilmazer, E. Bekaroglu, O. *Chem. Phys. Lett.* **1987**, *139*, 362. (e) Kobayashi, N.; Lever, A. B. P. *J. Am. Chem. Soc.* **1987**, 109, 7433. (f) Sielcken, O. E.; van Tilborg, M. M.; Roks, M. F.; Hendriks, R.; Drenth, W.; Nolte, R. J. M. *J. Am. Chem. Soc.* **1987**, *109*, 4261. (g) Ahsen, V.; Yilmazer, E.; Gurek, A.; Gul, A.; Bekaroglu, O.; Gebze, T. *Helv. Chim. Acta* **1988**, *189*, 2533. (h) Ahsen, V.; Yilmazer, E.; Ertas, M.; Bekaroglu, O. *J. Chem. Soc., Dalton Trans.* **1988**, 401. (i) Gasyna, Z.; Kobayashi, N.; Stillman, M. *J. Chem. Soc., Dalton Trans.* **1989**, 2397. (j) Sielcken, O. E.; Vandekuil, L. A.; Drenth, W.; Schoonman, J.; Nolte, R. J. M. *J. Am. Chem. Soc.* **1990**, *112*, 3086. (k) Kobayashi, N.; Opallo, M.; Osa, T. *Heterocycles* **1990**, *30*, 389. (l) Gurek, A.; Ahsen, V.; Gul, A.; Bekaroglu, O. *J. Chem. Soc., Chem. Commun.* **1991**, 3367. (m) Miyamoto, R.; Yamauchi, S.; Kobayashi, N.; Osa, T.; Ohba, Y.; Iwaizumi, M. *Coord. Chem. Rev.* **1994**, *132*, 57.

(2) Some representive ones: Kobayashi, N.; Osa, T. *Heterocycles* **1981**, *15*, 675. Thanabal, V.; Krishnan, V. *J. Am. Chem. Soc.* **1982**, *104*, 3463. Thanabal, V.; Krishnan, V. *Inorg. Chem.* **1982,** *21*, 3606. Richardson, N. M.; Sutherland, I. O.; Camilleri, P.; Page, J. A. *Tetrahedron Lett.* **1985**, *26*, 3739. Van Willigen, H.; Chandrashekar, T. K. *J. Am. Chem. Soc.* **1986**, *108*, 709. Gunter, M. J.; Johnston, M. R. *Tetrahedron Lett.* **1990**, *31*, 4801.

0002-7863/96/1518-1073$12.00/0

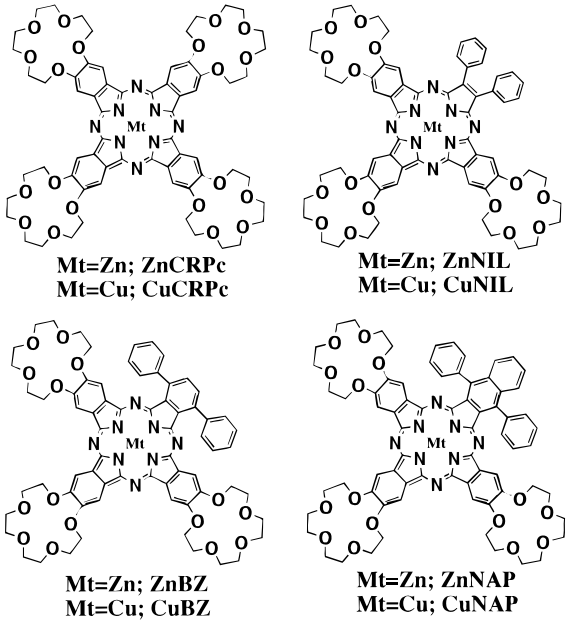

Figure 1. Structures and abbreviations of compounds appearing in this study.

Experimental Section

(i) Measurements. Electronic spectra were recorded with a Shimadzu VU-250 spectrophotometer, and magnetic circular dichroism (MCD) measurements were made with a JASCO J-720 spectrodichrometer equipped with a JASCO electromagnet that produced magnetic fields up to 1.53 T (T = tesla) with parallel and then antiparallel fields. Its magnitude was expressed in terms of molar ellipticity per tesla, $[\Theta]_M/10^4$ deg mol^{-1} dm^3 cm^{-1} T^{-1}. Fluorescence and excitation spectra were recorded with a Shimadzu RF-500 spectrofluorimeter with appropriate filters to eliminate scattered light. Fluorescence quantum yield (Φ_F) was determined by the use of H_2Pc and ZnPc ($\Phi_F = 0.60$ and 0.30, respectively)[3a] and quinine sulfate in 1 N H_2SO_4 ($\Phi_F = 0.55$ at 296 K)[3b,c] as standards. Data were obtained by a comparative calibration method with use of the same excitation wavelength and absorbance for ZnNIL, ZnBZ, and ZnNAP and the calibrants and the same emission energies. Fluorescence decay curves were obtained at 20 °C by a Horiba NAES-550 series, using combinations of glass filters and a monochrometer for monitoring the emission. The lifetimes were determined from the decay curves by the use of the least-squares method. All sample solutions for fluorescence measurements were purged with argon before measurement. 500 MHz ^{1}H NMR spectra were recorded with a Jeol GX-500 spectrometer using $CDCl_3$ or CD_2Cl_2 containing a small amount of CD_3OD as solvents. EPR spectra were collected with a Varian E4 spectrometer of samples in chloroform containing *ca.* 20% methanol at 77 K. The microwave frequencies were monitored by a Takedariken TR 5501 frequency counter with a TR-5023 frequency converter. TREPR spectra were observed for the lowest triplet states at 77 K and 0.5 μs after the laser pulse. The samples of 1×10^{-4} M in ethanol−chloroform (1:1 v/v) were excited at 600−650 nm by a Spectra Physics MOPO-710 broad band OPO laser pumped with a Spectra Physics GCR-170-10 Nd:YAG laser.

(ii) Materials. The so-called dicyanobenzo-15-crown-5 (2 equiv)[1e] and diphenylmaleonitrile,[4] 3,6-diphenylphthalonitrile,[5] or 2,3-dicyano-1,4-diphenylnaphthalene[6] (1 equiv) were fused in the presence of zinc- or copper acetate (0.5 equiv) at *ca.* 250−260 °C for 20−30 min. After cooling, the residue was washed well with water and methanol, and separation of the mixture was carried out using columns and preparative TLC on basic alumina. First, columns were eluted with CH_2Cl_2 and acetone to remove unreacted starting materials and Pc analogues containing one or two 15-crown-5 ether unit(s). In the subsequent preparative TLC using methanol and CH_2Cl_2−pyridine as the eluting solvents, the second green band was always collected, and after drying the residue was dissolved in CH_2Cl_2 and washed with water. The desired Pc analogues with three 15-crown-5 ether voids were collected from the organic layer. Elemental analyses and fast atom bombardment (FAB) mass data were satisfactory (Table 1). 500 MHz ^{1}H NMR data of monomeric zinc complexes in $CDCl_3$ (δ) are as follows. **ZnNIL**: 3.76 (s, 12H, CH_2), 3.83 (s, 12H, CH_2), 4.09 (s, 12H, CH_2), 4.55 (s, 4H, CH_2), 4.61 (s, 8H, CH_2), 7.55 (s, 2H, C*H*), 7.67 (s, 4H, C*H*), 8.32 (s, 4H, C*H*), 8.58 (s, 2H, C*H*), 8.79 (s, 4H, C*H*). **ZnBz**: 3.89 (s, 12H, CH_2), 3.94 (s, 12H, CH_2), 4.19 (s, 12H, CH_2), 4.44 (s, 12H, CH_2), 7.20−8.12 (m, 18H, C*H*). **ZnNAP**: 3.16−4.66 (m, 48H, CH_2), 6.92−8.70 (m, 20H, C*H*).

(iii) Computational Method. The deprotonated H_2NIL, H_2BZ, and H_2NAP (*i.e.*, NIL^{2-}, BZ^{2-}, and NAP^{2-}) structures were constructed by using standard phthalocyanine X-ray structural data[7] and by making the ring perfectly planar and adopting either D_{4h} (BZ) or C_{2v} (NIL and NAP) symmetry. Molecular orbital (MO) calculations were performed for the (pyrrole proton-) deprotonated dianionic species within the framework of the Pariser−Parr−Pople (PPP) approximation,[8a] where semiempirical parameters recommended in a recent book[8b] were employed. These were atomic valence state ionization potentials of 11.16 (carbon), 20.21 (central nitrogen), and 14.12 eV (imino nitrogen), together with atomic valence state electron affinities of 0.03 (carbon), 5.32 (central nitrogen), and 1.78 eV (imino nitrogen). The central nitrogen atoms were assumed to be equivalent, supplying 1.5 electrons each to the π-system. In addition, σ polarizability was taken into account according to Hammond.[8c] Resonance integrals were taken to be −2.48 (β_{CN}) and −2.42 eV (β_{CC}).[8b] Two-center electron repulsion integrals were computed by the method of Mataga and Nishimoto.[8d] The choice of configuration was based on energetic considerations, and all singly excited configurations up to 48 393 cm^{-1} were included.

Results and Discussion

(i) Cation Complexation Leading to Cofacial Dimers. Phthalocyanines with four crown-ether voids (MtCRPcs) are known to dimerize by encapsulating cations such as K^+ and Ca^{2+}. In these cases, the dimerization proceeds in a two-step three-stage process,[1e] and the first dimer is noncofacial while the last stage dimer is a rigidly cofacial eclipsed D_{4h} species. In electronic absorption spectroscopy, this was monitored as a decrease of the Q band peak of monomer (around 660−700 nm) and a concomitant increase of absorption intensity to shorter wavelength side (*ca.* 620−640 nm, the so-called dimer peak). A similar phenomenon was observed for MtNIL, MtBZ, and MtNAP in the present study. An example is shown in Figure 2, where the so-called monomer peak at 677 nm loses its intensity, while a new peak appears at 634 nm and develops, and the Soret band shifts to shorter wavelength with the increase of [Rb^+]. Considering that the blue-shift in the Q and Soret absorption bands in the Pc dimers and oligomers can be explained by an excitonic interaction[9] and that the EPR data for copper complexes in the presence of K^+ and Rb^+ will indicate the presence of two copper atoms in very close proximity, the final stage spectra can be ascribed to cofacial dimers. Moreover, the lack of a new peak to the longer

(3) Seybold, P. G.; Gouterman, M. *J. Mol. Spectrosc.* **1969**, *31*, 1.
(4) Cook, A. H.; Linstead, R. P. *J. Chem. Soc.* **1937**, 929.
(5) Mikhalenko, S. A.; Gladyr, S. A.; Luk'yanets, E. A. *J. Org. Chem. USSR (Engl. Transl.)* **1972**, *8*, 341.
(6) Kovshev, E. I.; Luk'yanets, E. A. *J. Gen. Chem. USSR (Engl. Transl.)* **1972**, *42*, 1584.
(7) Robertson, J. M.; Woodward, I. *J. Chem. Soc.* **1937**, 219: Barrett, P. A.; Dent, C. E.; Linstead, R. P. *J. Chem. Soc.* **1936**, 1719. Brown, C. J. *J. Chem. Soc. A* **1968**, 2488, 2494. Kirner, J. E.; Dow, W.; Scheidt, D. R. *Inorg. Chem.* **1976**, *15*, 1685.
(8) (a) Pariser, R.; Parr, R. G. *J. Chem. Phys.* **1953**, *21*, 466, 767. Pople, J. A. *Trans. Faraday Soc.* **1953**, 46, 1375. (b) Tokita, S.; Matsuoka, K.; Kogo, Y.; Kihara, K. *Molecular Design of Functional Dyes-PPP Method and Its Application*; Maruzen, Tokyo, 1990. (c) Hammond, H. *Theo. Thim. Acta* **1970**, *18*, 239. (d) Mataga, N.; Nishimoto, K. *Z. Phys. Chem. (Frankfurt am Main)* **1957**, *13*, 140.
(9) Dodsworth, E. S.; Lever, A. B. P.; Seymour, P.; Leznoff, C. C. *J. Phys. Chem.* **1985**, *89*, 5698.

Table 1. FAB Mass and Elemental Analytical Data

						anal.(%)					
						calcd			found		
compd	yield (%)	molecular formula	M_f for Mass	m/z[a]	M_f	C	H	N	C	H	N
ZnNIL	2.27	$C_{64}H_{64}O_{15}N_8Zn$	1249.85	1250	1250.64	61.46	5.16	8.96	61.27	5.37	8.73
CuNIL	1.78	$C_{64}H_{64}O_{15}N_8Cu$	1248.00	1248	1248.81	61.55	5.17	8.97	61.04	5.39	8.66
ZnBZ	2.65	$C_{68}H_{66}O_{15}N_8Zn$	1299.87	1301	1300.70	62.79	5.11	8.61	62.67	5.40	8.42
CuBZ	4.98	$C_{68}H_{66}O_{15}N_8Cu$	1298.02	1299	1298.87	62.88	5.12	8.63	62.48	5.29	8.27
ZnNAP	3.30	$C_{72}H_{68}O_{15}N_8Zn$	1349.87	1350	1350.76	64.02	5.07	8.30	63.61	5.38	8.05
CuNAP	2.57	$C_{72}H_{68}O_{15}N_8Cu$	1348.03	1348	1348.93	64.12	5.08	8.31	63.76	5.34	7.99

[a] Parent ion peak.

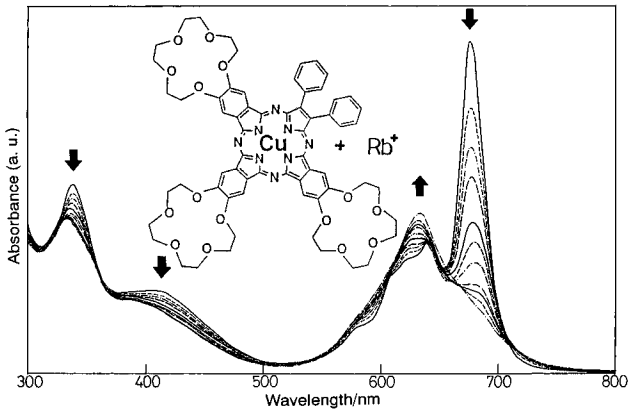

Figure 2. Change of absorption spectrum of CuNIL by the addition of CH_3COORb to 3 mL of a $CHCL_3$ solution in a 10-mm cell. The CH_3COORb in $CHCl_3$−MeOH (9:1 v/v) was added with a microsyringe; 30 μL were added in total. Arrows indicate the dirrection of spectroscopic change.

wavelength side of the monomer peak suggests theoretically[10] that the spectrum at the final stage is that of a cofacial and eclipsed configurated species.

In order to see the absorption intensity-cation concentration relationship, Figure 3 was obtained from experimental data such as those in Figure 2. In all cases, Rb^+ and K^+ are much more effective than Na^+ and Cs^+ with respect to the amount by which the intensity is altered. This is attributed to the size of cations.[1] K^+ and Rb^+ ions are sandwiched between two crown ether units, while Na^+ resides within the ether ring, and Cs^+ ion may be too large to be sandwiched.[11] The change almost saturates until [Rb^+] or [K^+]/[MtNIL, MtBz, or MtNAP] values reach roughly 2, in particular the change of the monomer peak is most sharp in the region of the above ratio of 0−1, indicating that encapsulation probably continues until the available sites are saturated, *i.e*. until two macrocyclic units bind three cations in a rigid eclipsed dimer.

Assuming the monomer−dimer equiliblium (eq 1) for the Rb^+ (or K^+)-triggered

$$n\mathrm{K}^+ + 2\mathrm{monomer} \overset{K}{\leftrightarrow} \mathrm{dimer\ K}^+_n \qquad (1)$$

spectroscopic change, the specific monomer and dimer concentrations were calculated by the method of West and Pearce[12] from the changes of intensity at the monomer peak, as a function of [K^+]. With use of this procedure, proof of dimer formation is obtained by plotting the calculated [monomer] against [dimer].[13] A region of slope 2 is the region where the dimerization process is taking place. Indeed, as revealed for ZnBZ at the bottom of Figure 3, a region with slope = *ca.* 2.0 continues untill [Rb^+]/[Pc analogues] = *ca.* 0.5, indicating that the monomer-dimer conversion proceeds with a very high formation constant (K for eq 1 with n=1, $(5.5 \pm 2.0) \times 10^9$ L^2 mol^{-2}) until two Pc-analogue units bind one cation. After this point, the slope of the plots approaches zero, especially beyond the region of [Rb^+]/[Pc analogues] > 1.5, revealing that dimerization is not occurring in this region. Taking the above information into account, it is easily conceivable that the linear Pc analog-cation-Pc analog complex formed in 0 < [Rb^+]/[Pc analog] < 0.5 range transforms into a cofacial dimer by further encapsulation of cations. Differing from the cases of MtCRPcs, however, clear isosbestic points were not observed. This may be due to the presence of several types of linear dimer, since when a cation is trapped by two crown ether units belonging to two different Pc analogues, several isomers are conceivable depending on which crown ether is used.

(ii) Electron Paramagnetic Resonance (EPR). Figure 4 shows the ESR spectra of copper derivatives in the presence or absence of cations in $CHCl_3$−MeOH (4:1 v/v) at 77 K. EPR spectra of Cu(II) ions have been intensively studied because of their relative simplicity due to d^9 configuration.[14] The spectra in the absence of any cations (for example curve a) are structureless and seem to be those of somewhat aggregated species.[15] Addition of excess sodium ions ([Na^+]/[Pc analog] = *ca.* 10−50) led to the development of more structural signal (curve b), basically similar to monomeric copper porphyrins and phthalocyanines. In this case, the Na^+ ions are trapped in the cavity of the crown ether moiety, and the resulting positive charge appears to keep the copper atoms separated and a clear, highly resolved EPR spectrum is obtained.

Addition of Rb^+ or K^+ ions to the solution of copper complexes induces dramatic changes in the EPR spectrum (curves c−f). In the $g = 2$ region, nitrogen super-hyperfine coupling is not seen but two strong perpendicular transitions accompanying the characteristic seven-line pattern due to two equivalent Cu(II) ions ($I = 3/2$) coupled together are yielded.[16] In the half-field region ($\Delta M = \pm 2$), seven equally spaced lines (90−115 G separation) are observed. These data provide unmistakable evidence for the formation of a symmetric dimeric molecule, and the absence of any EPR signal originating from a monomeric copper derivative can be attested to a high dimer formation constant. It seems difficult, in most cases, particularly

(10) Gouterman, M.; Holten, D.; Lieberman, E. *Chem. Phys*. **1977**, *25*, 139.

(11) The cavity size of 15-crown-5 is estimated from CPK models to be 1.7−2.2 Å. The ionic diameters of the cations used in this paper are Na^+ 1.90 Å, K^+ 2.66 Å, Rb^+ 2.96 Å, and Cs^+ 3.38 Å.

(12) Pearce, S.; West, W. P. *J. Phys. Chem.* **1965**, *69*, 1894.

(13) Nevin, W. A.; Liu, W.; Lever, A. B. P. *Can. J. Chem.* **1987**, *26*, 891.

(14) Manoharan, P. T.; Rogers, M. T. In *Electron Spin Resonance of Metal Complexes*; Yen, T. F., Ed.; Plenum: New York, 1979.

(15) Skorobogaty, A.; Smith, T. D; Dougherty, G.; Pilbrow, R. *J. Chem. Soc., Dalton Trans*. **1985**, 651 and several references cited therein.

(16) Smith, T. D.; Pilbrow, J. R. *Coord. Chem. Rev*. **1974**, *13*, 173. Eaton, S. S.; More, K. M.; Sawant, B. M.; Boymel, P. M.; Eaton, G. R. *J. Magn. Reson*. **1983**, *52*, 435. Thomson, C. *Q. Rev. Chem. Soc.* **1968**, *22*, 45. Kottis, P.; Lefebure, R. *J. Chem. Phys.* **1963**, *39*, 393.

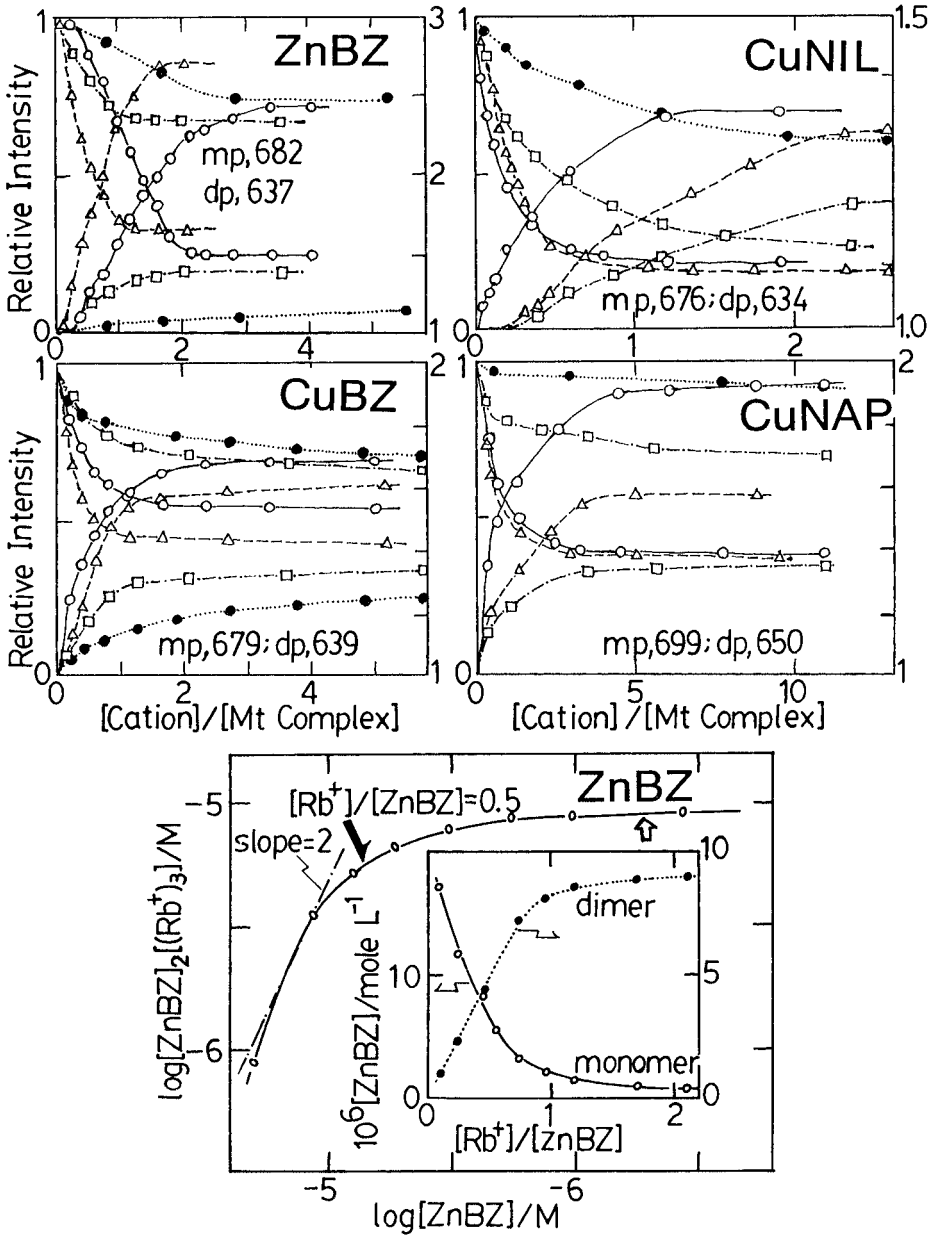

Figure 3. Dependence of absorbance of ZnBZ, CuBZ, CuNIL, and CuNAP on cation concentration for the so-called monomer peak (mp) and cofacial dimer peak (dp). Experiments were conducted as described in Figure 2. The wavelengths of mp and dp are shown in each figure, and the initial intensity without cation is set at unity. Curves going up with [cation] represent changes at dimer peaks and should be referred to the right-axis, while those going down are changes at monomer peaks and should be referred to the left-axis. Cations; Na^+ (●), Cs^+ (□), K^+ (○), and Rb^+ (△). Plots of log[ZnBZ] versus log($[ZnBZ]_2(Rb^+)_3$) for ZnBZ in $CHCl_3$ solution are shown at the botom. Experimental data such as those appeared in Figure 2 were analyzed with a computer program based on the approximation method of Pearce and West.[12] A line with a theoretical slope of 2 is added to show that dimerization is occurring in this region. An open arrow indicates the position of $[Rb^+]/[ZnBZ] = 1.5$. The inset shows the dependence of monomer and/or dimer concentration of ZnBZ on $[Rb^+]/[ZnBZ]$.

in the presence of Rb^+ or K^+, to envision the presence of linear oligomers in which Pcs are cofacial but joined to additional Pcs above or below the plane of the crown ether substituents (Scheme 1). For, if such species are present, a more complex specrum would be generated due to the superimposition of signals from "monomeric coppers" in Pcs pointed by arrows as shown in Figure 4 curves a and b and those from dimeric coppers as shown typically in curves e and f. In reality, however, such a spectrum is not recorded except for CuNAP plus saturated Na^+ system (curve h).

The behavior of CuNAP is slightly different from that of CuNIL and CuBZ. The latter two barely dimerize by the addition of Na^+ or Cs^+. However, in the presence of a large excess of Na^+ ($[Na^+]/[CuNAP] > ca.$ 1000) or Cs^+ ion ($[Cs^+]/[CuNAP] = ca.$ 100−150), CuNAP produces an EPR spectrum characteristic of a symmetric dimeric molecule (curves g and h). Although a trace of nitrogen super-hyperfine structure due to the monomeric molecule is still seen in the $g = 2$ region in the presence of saturated Na^+ (curve h), this high tendency for cofacial dimerization of CuNAP compared with CuNIL and CuBZ may be attributable to its large flat π-system. Generally, larger flat π-systems have higher tendency toward cofacial aggregation due to more intense $\pi-\pi$ hydrophobic interaction as seen typically in the comparison between phthalocyanines and naphthalocyanines.[17] The difference between CuBZ and CuNAP is only one benzene ring. Accordingly, it is interesting to note such a big difference between the two systems.

The EPR parameters for these spectra are collected in Table

(17) Tai, S.; Hayashi, N. *J. Chem. Soc., Perkin Trans.* **1991**, 1275. Tai, S.; Hayashi, N.; Katayose, M. *Prog. Org. Coatings* **1994**, *24*, 323.

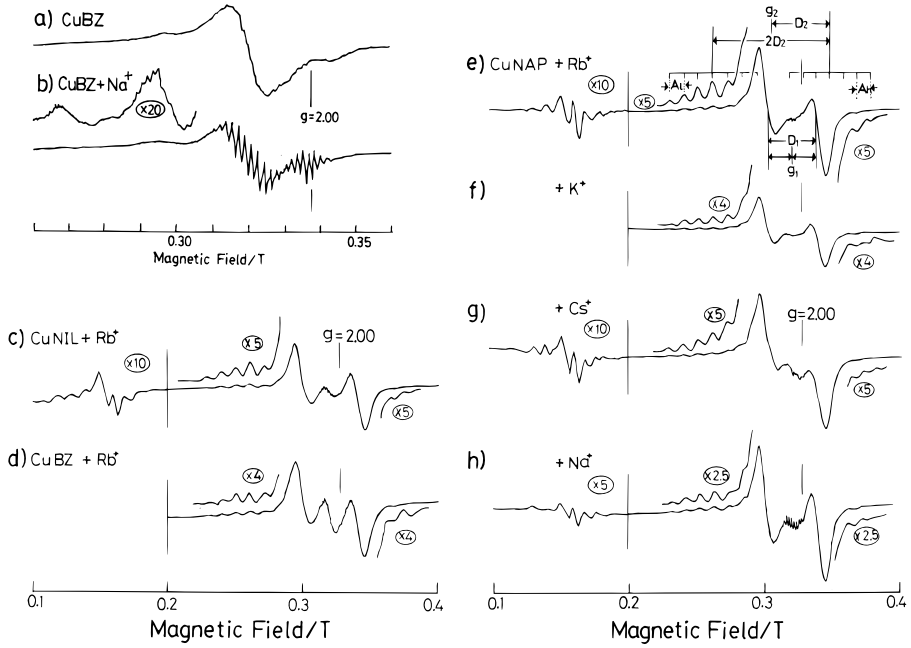

Figure 4. EPR spectra of copper complexes under various conditions in $CHCl_3$−MeOH (4:1 v/v) at 77 K. (a) CuBZ, (b) CuBZ + Na^+, (c) CuNIL + Rb^+, (d) CuBZ + Rb^+, and CuNAP with (e) Rb^+, (f) K^+, (g) Cs^+, and (h) Na^+. [Na^+]/[CuBZ] = *ca.* 100, [Rb^+]/[Cu complex] = *ca.* 5−10, [K^+]/[CuNIL] = 10, [Cs^+]/[CuNAP] = *ca.* 120−130, [Na^+]/[CuNAP] = *ca.* 1000, and [Cu complex]/M = *ca.* 0.001.

Table 2. Magnetic Parameters of Cation-Induced CuNIL, CuBZ, and CuNAP Cofacial Dimers[a]

compound	g_1	g_2	A_1,G	A_h,G	D_1,G	D_2,G	freq,MHz	Cu−Cu[b]dist, Å
$[CuNIL]_2(Rb^+)_3$	2.049	2.151	105	98	369	424	9177	4.131
$[CuBZ]_2(Rb^+)_3$	2.057	2.155	101	114	352	418	9176	4.154
$[CuNAP]_2(Rb^+)_3$	2.050	2.153	106	102	344	414	9175	4.166
$[CuNIL]_2(K^+)_3$	2.051	2.142	101	89	335	424	9178	4.126
$[CuNIL]_2(Cs^+)_3$		2.148	106	104		421	9180	4.139
$[CuNIL]_2(Na^+)_3$	2.053	2.142	98	92	355	417	9176	4.149

[a] See Figure 4e for definition of parameters. [b] Calculated via $r^3 = (1.39 \times 10^4) \times g_2/D_2$, where D is in G and r is in Å.

Scheme 1

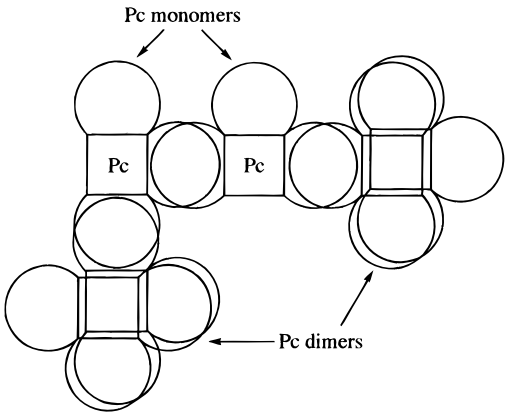

2, having been evaluated by standard procedures.[18] The calculated Cu−Cu distance is 4.12−4.17 Å and is not sensitive to the sizes of cations added. Since the diameter difference between Na^+ and Cs^+ ions is 1.48 Å,[11] the above insensitivity of the Cu−Cu distance with the cation size suggests that two crown ether units sandwiching cations are not necessarily in parallel with each other (they may be opened outward looking from the center of the macrocycles particularly when larger cations are trapped).

(iii) ^{1}H Nuclear Magnetic Resonance (NMR) Spectra. The ^{1}H NMR spectra of zinc complexes were recorded in both the presence and absence of cations. Figure 5 shows those of ZnNIL. The spectrum of the mononuclear species in the absence of cations (Figure 5B) is relatively simple and could be assigned as shown, based on the integrated ratios of protons and taking the ring current anisotropy of the azamacrocyclic core into account. Of crown ether protons, those of **1** and **1′**, closest to the macrocyclic core, appeared at two positions (δ = 4.55 and 4.61 ppm, respectively) because of chemical inequivalency due to the presence of phenyl rings. Comparing the positions of the aliphatic proton resonance in ZnNIL (*ca.* 3.8−4.6 ppm) and ZnCRPc (*ca.* 3.7−4.3 ppm),[1e] the ring current in the former appears to be a little larger than the latter. Qualitatively, this phenomenon might be explained by a "descent-in-symmetry" model.[19] It is known that the inner 16-membered ring contributes most to the aromaticity of porphyrinic compounds. If we consider that the porphyrinic structure is made by deforming an idealized 16-membered cyclic polyene with the D_{16h} symmetry, the ring current in porphyrins appears to be smaller than that in polyene due to "bumps" in the ring, such as acute corners and the presence of heteroatoms. Since the ring current seems to decrease with increasing of interference along this polyene, the ring current of ZnNIL appears to be larger than that in ZnCRPc. In accordance with this argument, it is already suggested that the ring current in naphthalocyanine is smaller than in Pcs.[20] That is, regarding that fused benzene rings are interferences to the ring current of polyene, there are three benzenes in ZnNIL while there are four in ZnCRPc.

The addition of RbCl to a solution of ZnNIL ([Rb^+]/[ZnNIL]

(18) (a) Chikira, M.; Yokoi, H.; Isobe, T. *Bull. Chem. Soc. Jpn.* **1974**, *47*, 2208. (b) Chikira, M.; Kon, H.; Hawley, R. A.; Smith, K. M. *J. Chem. Soc., Dalton Trans.* **1979**, 246 and some references cited therein. (c) Chasteen, N. D.; Belford, R. N. *Inorg. Chem.* **1970**, *9*, 169.

(19) Ceulemans, A.; Oldenhof, W.; Wahrand, C. G.; Vanquickenborne, L. G. *J. Am. Chem. Soc.* **1986**, *108*, 1155.

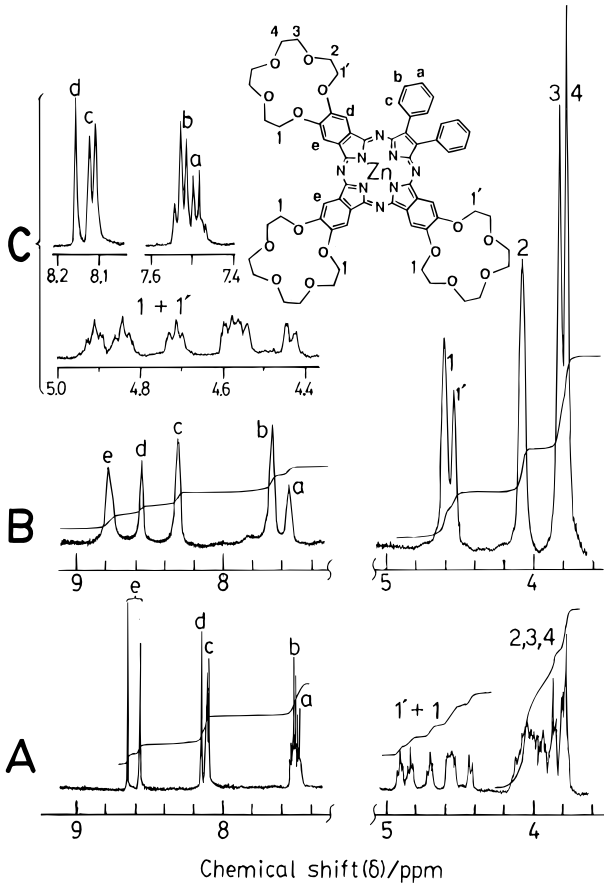

Figure 5. 500 MHz proton NMR spectra of (A) $[ZnNIL]_2(Rb^+)_3$ and (B) ZnNIL in CD_2Cl_2. Curves (C) are expansion of (A).

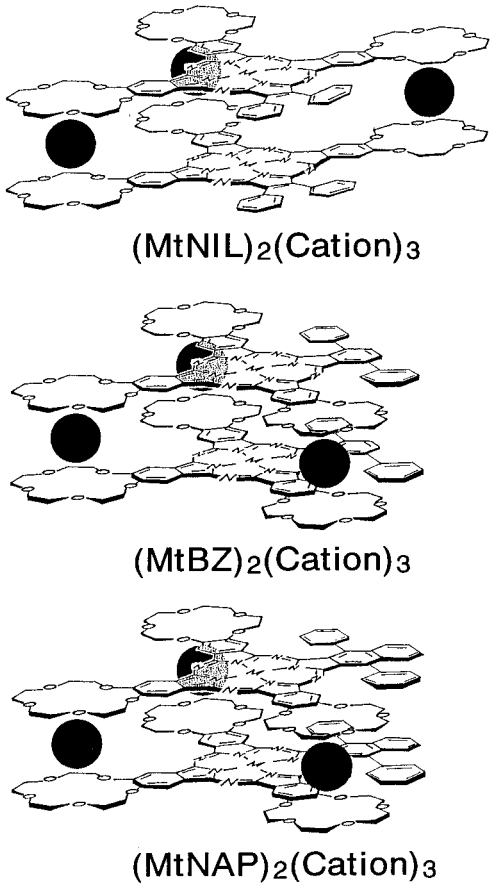

Figure 6. Proposed structures for the cation-induced dimers of MtNIL, MtBZ, and MtNAP. Solid circles indicate cations such as Rb^+ and K^+. Although not well represented, the phenyl rings would be tilted from the macrocyclic plane.

= *ca.* 2−10) increases the complexity in the whole region (Figure 5A and C), and the signals spread out. These data are consistent with cofacial dimer formation. Aromatic proton resonances shift upfield slightly and become sharper, due probably to the restricted rotaion of the $O-CH_2CH_2-O$ groups or to the greater rigidity imposed by encapsulation of the cations. While the aliphatic protons are either unshifted (protons **2**, **3**, and **4**) or shifted to downfield only slightly (protons **1** and **1′**). These resonance shifts are consistent with the prediction by calculation on the Pc ring current effect,[21] assuming the interplanar distance is *ca.* 4.1−4.2 Å.

As shown in the above "Materials" section, the NMR signals of ZnBZ and ZnNAP were not well resolved compared with those of ZnNIL even in the absence of cations. It is conceivable that these compounds are, to some extent, in aggregated forms in the NMR concentration range, as suggested by the ESR signal in the absence of cations (concentrations for ESR and NMR measurements are approximately the same order, *i.e.*, 10^{-4}−10^{-3} M). In the presence of Rb^+ ($[Rb^+]/[ZnBZ]$ = *ca.* 6); however, each singlet ether proton resonance of ZnBZ splits into triplets, suggesting and consistent with the formation of cofacial dimers (Figure 6).

One referee pointed out that the NMR shown in Figure 5A might be consistent with a dimeric species containing only one cation opposite the two phenyl substituents. We would rather like to deny this possibility for the following two reasons: (i) If two ligands have only one cation, the fixation of the dimer structure is evidently impossible. Under such a circumstance, a line width of NMR signals would be broader than that of monomers due to the presence of various types of linear dimers. However, the line width of dimers in the presence of Rb^+ (Figure 5A) is much sharper than in its absence (Figure 5B). (ii) It is already well-known and substantiated that the ESR spectra such as those shown in Figure 4 curves c−h are not produced unless two equivalent copper(II) ions are in very close proximity.[18a,b] In particular, the seven-line pattern in the half-field ($\Delta M = \pm 2$) region is not observed if one copper skews from directly above the other.

(iv) Electronic Absorption and MCD spectra. In Figures 7 and 8 are shown the electronic absorption and MCD spectra of ZnNIL and ZnNAP, and Table 3 summarizes the UV−visible absorption and MCD data of all compounds in this study. The electronic absorption spectra of tribenzotetraazaporphyrins[22] and tribenzomononaphthotetraazaporphyrins[22b,23] have seldomly been reported and their MCD spectra are, of course, not found in the literature. The absorption spectrum of monomeric ZnNIL (Figure 7) is quite different from that of general MtPcs in that four-peak Q bands are seen at 686, 638, 625, and 582 nm due to the lowering of molecular symmetry to C_{2v}. From the interpeak energy difference (ΔE_p), the bands at 686 and *ca.* 638 nm ($\Delta E_p = 1117$ cm^{-1}) are considered to belong to one couple and those at 625 and 582 nm ($\Delta E_p = 1182$ cm^{-1}) to a second couple. The ΔE_p difference of *ca.* 1100−1200 cm^{-1} is appropriate as the spacing of vibrational bands in Pc com-

(20) Janson, T. R.; Kane, A. R.; Sullivan, J. F.; Knox, K.; Kenney, M. E. *J. Am. Chem. Soc.* **1969**, *91*, 5210. Kane, A. R.; Yalman, R. G.; Kenney, M. E. *Inorg. Chem*. **1968**, *7*, 2558. Koyama, T.; Suzuki, T.; Hanabusa, K.; Shirai, H.; Kobayashi, N. *Inorg. Chim. Acta* **1994**, *218*, 41.

(21) Johnson, C. E.; Bovey, F. A. *J. Chem. Phys.* **1958**, *29*, 1012.

(22) (a) Elvidge, J. A.; Linstead, R. P. *J. Chem. Soc.* **1955**, 3536. (b) Kobayashi, N.; Kondo, R.; Nakajima, S.; Osa, T. *J. Am. Chem. Soc.* **1990**, *112*, 9640.

(23) Ikeda, Y.: Konami, H, Hatano, M: Mochizuki, K. *Chem. Lett.* **1992**, 763.

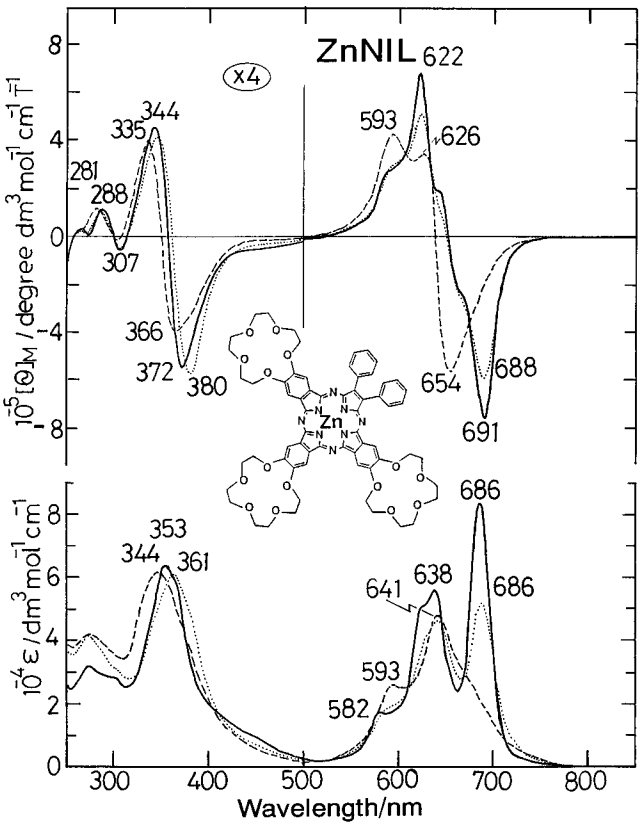

Figure 7. UV−visible absorption (bottom) and MCD (top) spectra of ZnNIL monomer (solid lines), ZnNIL-Rb^+-ZnNIL linear dimer (dotted lines), and $[ZnNIL]_2(Rb^+)_3$ cofacial dimer (broken lines) in $CHCl_3$.

pounds.[24] The apparently intense peak at 638 nm is then considered to be the Q_{0-1} vibrational peak which was strengthened by the overlap of a peak at 625 nm, and the weak 582 nm peak is the $Q_{0-1}1$ vibrational component of the band at 625 nm. Reflecting a big splitting of the Q_{0-0} band (1423 cm^{-1}), the total Q bandwidth of ZnNIL (*ca.* 3500 cm^{-1}) is much broader than that of usual ZnPc (for example, *ca.* 2600 cm^{-1} in ZnCRPc).[1e] In the Soret (or B1 + B2) band region, four bands are detected at 364 (sh), 353, 303, and 273 nm, in addition to a small curvature between *ca.* 430 and 470 nm. In the case of general MtPcs with D_{4h} symmetry, the B1 and B2 bands appear at *ca.* 300−400 nm[1i,25] with separations of *ca.* 2000−7000 cm^{-1}, together with a weaker band at *ca.* 260−300 nm named the N band.[24a] Thus, a shoulder at 364 and a peak at 353 nm appear to be resulted of the complex superimposition of four bands generated by the splitting of both the B1 and B2 bands, while two peaks at 273 and 303 nm are considered to correspond to the split components of the N band. The 303 nm peak is too small to assign to the split components of the B2 band. Because of the low intensity, the assignment of the curvature between *ca.* 430 and 470 nm is ambiguous. If we take into account that the B1 band of NiCRPc was found at 410 nm,[1i] this moiety may correspond to a split component of B1 band. However, since the alkoxy group-substituted Pcs commonly show a curvature in this region, and since this band intensifies with an increasing number of alkoxy groups on Pc periphery,[1e,i] this moiety may be ascribed to a transition involving ether oxygen lone pairs, such as n-π^*. The spectroscopic behavior of CuNIL resembles that of ZnNIL.

The electronic spectrum of ZnNAP is different from that of ZnNIL in the Q band region but close to that of ZnPc. In this way, the extent of departure from D_{4h} symmetry seems small in this compound. However, the effect of fusion of a naphthalene ring can be seen in the Q band region. In fact, the band to the longest wavelength with a peak at 698 nm is not symmetrical and suggests that at least one weak band is buried in the longer wavelength side of this peak. Although not shown, this phenomenon was more clearly detected in the spectra of CuNAP. In this case, a shoulder appeared at 710 nm with ϵ = 125 800, together with an intense (ϵ = 137 800) peak at 699 nm (Table 3). The splitting energy of this Q_{0-0} band in ZnNAP (roughly *ca.* 280 cm^{-1}) is much smaller than that in ZnNIL (*ca.* 1420 cm^{-1}). Another interesting characteristic on the Q band is that, of the split two peaks, the one at lower energy is stronger for MtNIL while weaker for MtNAP. The large difference in the splitting of the Q bands and the difference in the relative intensity of the split Q bands observed for MtNIL and MtNAP will be reproduced later by MO calculations. The apparently unsplit Soret (B1 + B2) and N bands appeared at 351 and 296 nm, respectively, and they are very close to those of ZnBZ (353 and 292 nm). From the standpoint of symmetry, these bands also should contain two bands each. The lack of splitting in these bands implies that the splitting energies in the Soret and N bands are also small, as in the Q band.

The spectra of ZnBZ and CuBZ are very close to those of MtPcs with D_{4h} symmetry, since their π-conjugated system has D_{4h} symmetry. However, because of the low symmetrical distribution of substituent groups on Pc periphery, the Q_{0-0} bands of these compounds are less symmetrical with respect to their peak positions, and in the case of CuBZ, a weak shoulder is seen to the red (685 nm) of the main Q_{0-0} band at 679 nm (Table 3, the splitting energy = *ca.* 130 cm^{-1}).

On cofacial dimer formation ($[Rb^+]$/[ligand] = *ca.* 4−6), the band due to the monomer species decreases in intensity, while there is growth in the band due to the cofacial dimeric species.[9,10] That is, the Q_{0-0} band of monomers decreased and concomitantly a broad new peak developed to the blue, as shown in Figure 2 for CuNIL system. This phenomenon can be explained qualitatively as a result of the interaction among excited states as follows.[10] Namely, if we have nondegenerate dipolar allowed states X, Y on moiety A interacting with a similar pair X′, Y′ on moiety B, the nature of exciton coupling depends on the detailed dimer geometry. However, to a first approximation, the four states interact in pairs. Thus, the four resulting dimeric states are roughly of the form X ± X′ and Y ± Y′ except coefficients. In the case of a cofacial eclipsed dimer, the expected geometry would have the transition dipoles of two pairs of states, say X and X′ and Y and Y′, perpendicular to the vector $\boldsymbol{R}$ between the centers; the allowed exciton state may then be unshifted or blue shifted. This accounts for the presence of two bands in each of the Q, B1, B2, and N bands, although the splitting of bands is not clearly seen in the actual spectra. The exciton splitting energies estimated as twice the difference between the Q band absorption of dimers and the average energy of the split Q bands of monomers are 567, 749, 2176, 1924, 2445, and 2497 cm^{-1} for ZnNIL, CuNIL, ZnBZ, CuBZ, ZnNAP, and CuNAP, respectively, indicating that the exciton energy increases with increasing molecular size. Since the center−center distance of these dimers is the same, this fact further indicates that transition dipoles become larger with increasing

(24) (a) Stillman, M. J.: Nyokong, T. *Phthalocyanines-Properties and Applications*; Leznoff, C. C., Lever, A. B. P., Eds.; VCH Publishers: Weinheim, Germany, New York, 1989; Chapter 3. (b) Luk'yanets, E. A. *Electronic Spectra of Phthalocyanines and Related Compounds*; Tcherkassy: Moscow, 1989. (c) Kobayashi, N. *Phthalocyanines-Properties and Applications*; Leznoff, C. C., Lever, A. B. P., Eds.; VCH Publishers: Weinheim, Germany, New York, 1993; Vol. 2, Chapter 3. (d) Kobayashi, N.; Nakajima, S.; Osa, T. *Inorg. Chim. Acta* **1993**, *210*, 131.

(25) Nyokong, T.; Gasyna, Z.; Stillman, M. J. *Inorg. Chem.* **1987**, *26*, 1087. Ough, E.; Nyokong, T.; Creber, K. A. M.; Stillman, M. J. *Inorg. Chem.* **1988**, *27*, 2724.

Table 3. Electronic Absorption and MCD Data in Chloroform

compd	electronic absorption l/nm($10^{-4}\epsilon$/M^{-1} cm^{-1})				MCD l/nm ($10^{-5}[\Theta]_M$/deg dm^3 mol^{-1} cm^{-1} T^{-1})			
ZnNIL	686(8.50)	638(5.73)	625(5.22)sh	582(1.76)	691(−7.61)	622(6.68)	372(−1.35)	344(1.12)
	364(5.57)sh	353(6.47)	303(2.85)	273(3.28)	307(−0.14)	288(0.31)		
$[ZnNIL]_2(Rb^+)_3$	641(5.08)	593(2.66)	344(6.28)	272(4.34)	654(−5.62)	626(3.46)	593(4.32)	366(−0.95)
					335(1.01)	305(−0.04)	281(0.30)	
CuNIL	677(6.72)	641(2.85)	624(2.51)sh	338(4.08)	687(−7.58)	673(3.96)	657(−0.39)	612(2.03)
	292(3.45)	276(3.40)			352(−0.48)	321(0.33)	287(0.24)	
$[CuNIL]_2(Rb^+)_3$	634(3.54)	332(3.25)	287(3.29)	274(3.47)	651(−2.22)	614(1.61)	348(−0.28)	323(0.25)
					287(0.18)			
ZnBZ	678(9.22)	613(1.67)	353(4.48)	292(2.39)	691(−13.2)	675(9.69)	616(2.67)	362(−0.77)
	279(2.60)				333(0.43)			
$[ZnBZ]_2(Rb^+)_3$	673(2.73)	637(3.98)	342(3.61)	290(2.28)	693(−2.84)	678(0.14)	651(−2.38)	632(3.41)
	278(2.76)				368(−0.32)	330(0.43)		
CuBZ	685(6.25)sh	679(6.85)	616(1.75)	341(3.81)	694(−7.37)	678(5.24)	617(2.10)	351(−0.52)
	274(4.50)				324(0.42)			
$[CuBZ]_2(Rb^+)_3$	698(2.36)sh	677(2.83)	640(2.93)	337(3.03)	700(−3.07)	681(0.30)	659(−1.02)	620(2.19)
	271(4.47)				350(−0.37)	323(0.37)		
ZnNAP	698(11.53)	628(2.59)	351(5.97)	296(4.17)	712(−14.9)	698(11.57)	670(2.12)	634(2.62)
					360(−0.55)	334(0.42)		
$[ZnNAP]_2(Rb^+)_3$	694(3.57)	649(4.27)	345(5.53)	293(4.45)	712(−1.99)	676(−1.69)	638(2.31)	358(−0.29)
					333(0.36)	284(0.12)		
CuNAP	710(12.58)sh	699(13.78)	631(3.94)	418(2.25)	716(−15.84)	700(10.81)	636(3.24)	348(−0.97)
	342(5.59)	299(6.44)			322(0.51)	293(0.24)	275(−0.09)	
$[CuNAP]_2(Rb^+)_3$	693(5.19)	650(5.80)	415(2.05)	339(6.62)	695(−2.06)	637(2.69)	350(−0.52)	323(0.37)
	297(6.12)				290(0.19)	272(−0.07)	259(0.05)	

molecular size of constituent monomers. In accordance with this result, the Q band intensifies in the order tetraazaporphyrin, Pc, naphthalocyanine, and anthracocyanine.[24c,d] In the cases of ZnCRPc and CuCRPc,[1e] these values were 1954 and 1910 cm^{-1}, respectively. The Soret band also shifts to the blue with concomitant decrease in absorption coefficient. Although the shift is only 3−11 nm in nm unit, this is not small in cm^{-1} unit (*ca.* 260−910 cm^{-1}).

MCD spectra of monomeric species, *i.e.*, in the absence of cations, can be interpreted at least theoretically as the superimposition of Faraday *B*-terms,[26] showing minima and maxima corresponding roughly to the absorption maxima, because no degenerate states are included (however, MtBZs show a Faraday *A*-term-like pattern due to the D_{4h} symmetry of the chromophore). The dispersion type (the *A*-term-like) MCD curves corresponding to the Q_{0-0}, Soret, and N bands are produced as the superimposition of adjacent interacting *B*-terms. This is most clearly seen in the spectrum of ZnNIL (Figure 7). MCD troughs are observed at 691, 372, and 307 nm corresponding to the absorption peaks at 686, 364 (sh), and 303 nm, respectively, while MCD peaks are at 622, 344, and 288 nm associated with the absorption peaks at 622, 353, and 273 nm, respectively. The curvature seen in 400−500 nm of the spectrum of ZnNIL and in 370−500 nm of that of ZnNAP indicates that there are indeed weak transitions in these regions. These are perhaps associated with either the split components of the B1 band in MtPcs with D_{4h} symmetry or transitions involving ether oxygen lone pairs, as mentioned for the spectrum of ZnNIL.

By the addition of Rb^+ required to make cofacial dimers, the MCD band also shifted to the blue with a concomitant decrease in intensity. A small negative MCD trough detected at the Q band to the longest wavelength suggests that a small amount of monomeric species may be still present in the solution (not explicit for ZnNIL but clearly seen for ZnNAP at 712 nm). The positions of the inflection points of dispersion curves are close to the absorption peaks of the main Q, B1 + B2, and N bands. However, these are perhaps being produced as the superimposition of Faraday *B*-terms of opposite signs, although

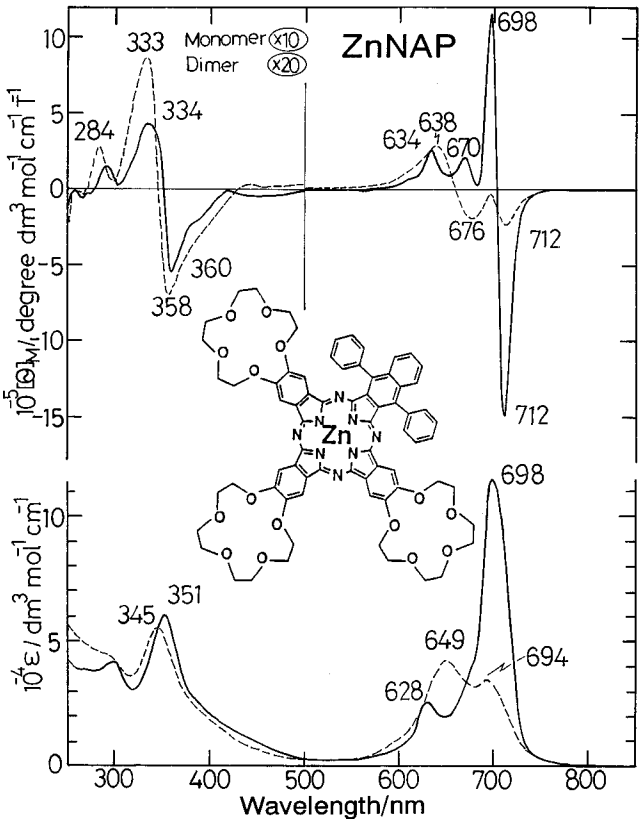

Figure 8. UV−visible absorption (bottom) and MCD (top) spectra of ZnNAP monomer (solid lines) and $[ZnNAP]_2(Rb^+)_3$ cofacial dimer (broken lines) in $CHCl_3$.

no one can rule out the possibility of the Faraday *A*-terms completely. According to Kaito *et al.*[27] who constructed the "apparent" *A*-term using band shape functions assuming the damped oscillator model, the dispersion type curve could easily be produced corresponding to the seemingly single broad absorption peak when the two bands of opposite signs were separated by 1000 cm^{-1} and the bandwidth at half height (Γ)

(26) Tajiri, A.; Winkler, J. *Z. Naturforsh.* **1983**, *38a*, 1263.

(27) Kaito, A.; Nozawa, T; Yamamoto, T.; Hatano, M; Orii, Y. *Chem. Phys. Lett.* **1977**, *52*, 154.

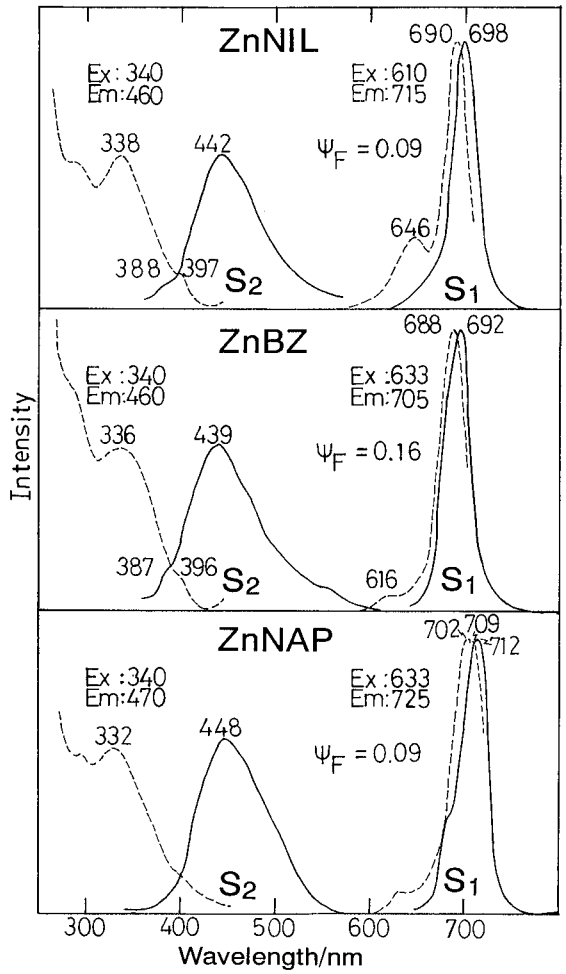

Figure 9. Fluorescence emission (solid lines) and excitation spectra (broken lines) of ZnNIL (top), ZnBZ (middle), and ZnNAP (bottom) in $CHCl_3$. In each species, there is no intensity relationship between S_1 and S_2 emissions. Excitation wavelengths and emission wavelengths used to record excitation spectra are shown. Φ_F is quantum yield. The absorbance at the excitation wavelengths was always less than 0.05.

was set at 2000 cm^{-1}, *i.e.*, when the separation of the two bands are a half of Γ. In this particular case, the Γ of the resultant absorption band became roughly *ca.* 3000 cm^{-1} and the energy difference between MCD trough and peak (Δ*E*(trough-to-peak)) reached *ca.* 1600 cm^{-1}. This means that the "apparent" *A*-term is of course produced from two *B*-terms of opposite signs, if their separation is less than half of the bandwidth at half height. In the case of usual MtPc, the Γ values of monomers are roughly *ca.* 700−1500 cm^{-1} in the Q band and 1200−2000 cm^{-1} in the Soret band regions (in general, the bandwidth of the spectra of aromatic compounds broadens the higher the energy of the bands).[28] In our experimental spectra of cofacial dimers, Γ and Δ*E*(trough-to-peak) values in the Q band region are *ca.* 1200−1400 and 680−1300 cm^{-1}, while those in the Soret band are *ca.* 3300−4800 and 2100−2500 cm^{-1}, respectively. If we admit that the Q and Soret bands of C_{2v} compounds theoretically involve two and four transitions (the split B1 and B2 components), respectively, the above data strongly suggest that Faraday *A*-term-like MCD spectra can be produced as the superimposition of *B*-terms in the spectra of MtNIL and MtNAP.[29]

(v) Emission Spectra. We measured the fluorescence emission and excitation spectra of three zinc complexes. The spectra are shown in Figure 9, and the obtained values of quantum yield (ϕ_F) and lifetimes (τ) are listed in Table 4. All compounds exhibited the so-called S_1 and S_2 emission, as have been found commonly for alkoxy group-substituted Pcs.[1e,30] The S_2 emission is much broader than the S_1 emission, and the band shape is similar to that observed for tetraneopentoxy group-substituted Pcs.[30] In each case, the Stokes shift of the S_1 emission is very small, while that of the S_2 emission is generally large. In the case of the S_1 emission of ZnNIL, the corresponding excitation spectrum indicates that the emission occurs mainly from the lower energy component of the split Q band, while the two peaks (at 702 and 709 nm) in the S_1 excitation spectrum of ZnNAP substantiate experimentally that the Q band of this species is split and therefore that the molecular symmetry of ZnNAP is lower than D_{4h}.

Table 4. Quantum Yields (ϕ_F) and Lifetimes (τ) of ZnNIL, ZnBz, and ZnNAP in Deaerated Chloroform at Room Temperature[a]

	S_1		S_2		
compd	ϕ_F	τ/ns	$10^3\phi_F$	τ_1/ns(%)	τ_2/ns(%)
ZnNIL	0.09	2.23	8.87	5.94(29.4)	19.4(70.6)
ZnBZ	0.16	3.12	6.54	3.28(48.5)	25.5(51.5)
ZnNAP	0.09	3.46	8.49	3.31(27.5)	26.2(72.5)

[a] Emission wavelengths for recording S_1 and S_2 excitation spectra were 715, 705, and 725 nm and 460, 460, and 470 nm, respectively, in the order ZnNIL, ZnBZ, and ZnNAP. Because of solution instability, ϕ_F values of S_2 emission were obtained using the first spectra recorded after deaeration.

(28) Mack, J.; Stillman, M. J. *J. Am. Chem. Soc.* **1994**, *116*, 1292.

(29) Deconvolution of the spectroscopic envelope can give reliable results if both the absorption and MCD spectra are fitted with the same or very similar band center and bandwidth parameters. In fact, to date many absorption and MCD spectra have been analyzed by band deconvolution and it has been successful in analysing transitions which had been postulated by MO calculations or in finding a new degenerate excited state (some representative ones are refs 25, 28, and follows: (a) Browett, W. R.; Gasyna, Z.; Stillman, M. J. *J. Am. Chem. Soc*. **1988**, *110*, 3633. (b) Gasyna, Z.; Kobayashi, N.; Stillman, M. J. *J. Chem. Soc., Dalton Trans*. **1989**, 2397. (c) Ough, E. A.; Stillman, M. J.; Creber, K. A. *Can. J. Chem*. **1993**, *71*, 1898. (d) Ough, E. A.; Stillman, M. J. *Inorg. Chem*. **1994**, *33*, 573). It is important to underscore the fact that both sets of spectra (that is, the associated absorption and MCD spectra recorded from the same solution) must be fitted with the same set of parameters. Of course band deconvolution has to be carefully performed to the extent that removal of only one of the fitted bands results in fits that clearly do not realistically account for all the intensity in one or the other of the two spectral envelopes. Accordingly, we made a program so that the fitting procedures are based upon the assumption that the bandwidths and band centers will be identical in both the absorption and MCD spectra. As introduced in previous papers (refs 25, 28, and above), whenever an *A*-term was used, a *B*-term was also added in, and this *B*-term had exactly the same parameters as the *A*-term. This home made program uses least-squares and Simplex iteration routines to obtain the best fit between calculated and experimental data by varying the band centers and bandwidths of the Gaussian-shaped bands that are assumed to make up the spectra. Also, we took the recently identified result into account that the bandwidth generally becomes larger the higher the energy of the band.[28] When *A*-terms dominate the MCD spectrum, the band assignment is straightforward. However, since in the present case, both the ground and excited states are nondegenerate, the spectra were deconvoluted entirely with Gaussian-shaped *B*-terms. Analysis was performed for dimeric spectra of copper complexes, since their EPR spectra in the presence of Rb^+ clearly indicated that they exist as dimers. For CuNIL, CuBZ, and CuNAP, 23, 22, and 22 components are required, respectively. The "apparent" *A*-term-like, dispersion curves are reproduced at *ca.* 15 670 and 29 860 cm^{-1} for CuNIL, 15 690 and 29 650 cm^{-1} for CuBZ, and 15 080 and 29 530 cm^{-1} for CuNAP, supporting approximate red-shifting with increasing molecular size. The inversion of the Q band position between CuNIL and CuBZ would be ascribed to the large splitting of the Q band of the former. We dared to deconvolute the MCD of the above derivatives introducing *A*-terms also. In this case, *A*-terms are required at 15 720 (band half width = 508 cm^{-1}) and 29 919 (1456) cm^{-1} for CuNIL, 15 505 (899) and 29 857 (1328) cm^{-1} for CuBZ, and 15 181 (893) and 29 506 (1287) cm^{-1} for CuNAP. As reiterated in the text, *A*-terms are not present theoretically. However, if this were the case, this then means that the MCD spectra of cofacial C_{2v} species are insensitive to the molecular symmetry of constituting monomers. We believe that no one can deny this possibility completely because the spectroscopic shape is similar among species, and the spectra contain little structures (see for example the Q band region).

(30) Kobayashi, N.; Lam, H.; Nevin, W. A.; Leznoff, C. C.; Koyama, T.; Monden, A.; Shirai, H. *J. Am. Chem. Soc.* **1994**, *116*, 879.

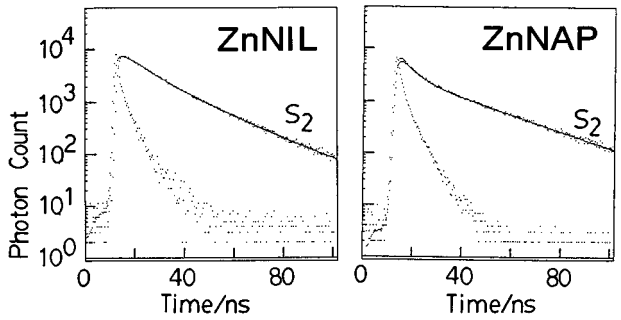

Figure 10. S_2 fluorescence decays of ZnNIL and ZnNAP in deaerated $CHCl_3$ and their typical biexponential fit. For lifetimes (τ), see Table 4.

Concerning the quantum yield of S_1 fluorescence emission, it is known already that it decreases with lowering of molecular symmetry.[31] Indeed, the ϕ_F values are fairly small compared with ϕ_F (= 0.30) of ZnPc without substituent groups.[3] Although the π-conjugated system of ZnBZ is approximated by D_{4h} symmetry, its ϕ_F value is already about half of that of ZnPc (0.30), suggesting that the substituent groups on ZnBZ affects the effective symmetry.

Knowledge on S_2 emission of Pcs is still very limited. According to two papers so far published,[30,32] ϕ_F values of S_2 emission are of the order of 10^{-4} and in order to obtain a good fit of the decay curves, double-exponential functions are always required. This holds in the present systems also. Figure 10 shows fluorescence decay of ZnNIL and ZnNAP and their biexponential fits. Two components, one with τ = subnanosecond and the other with τ = 19−27 ns were required. Since the latter values are fairly larger for states with a singlet multipticity,[33] the S_2 emission may be originating in ligand-centered triplet states, such as $\pi-\pi^*$.

According to hitherto accummulated data on porphyrins,[34] porphyrin dimers emit much more weakly than monomers, and since the dimer formation by the addition of certain cations was suggested in our systems also, we pursued the S_1 emission intensity as a function of $[Rb^+]$ and $[Na^+]$. The results are shown in Figure 11. Addition of Rb^+ to zinc monomers leads to quenching, and its behavior corresponds almost exactly to that in the absorption study. Quenching is particularly marked in $0 < [Rb^+]/[\text{ligand}] < 1$ region, while above $[Rb^+]/[\text{ligand}]$ = *ca.* 1.5 or 2, the emission intensity becomes almost constant, supporting, and consistent with two macrocycles approaching in the former region and that cofacial dimers in the latter region emit most weakly. Note here again that the dimerization is the process in which two macrocycles are being linked by a cation, so the $0 < [Rb^+]/[\text{ligand}] < 1$ region corresponds to this process, while the $[Rb^+]/[\text{ligand}] >$ *ca.* 1.5 or 2 region is the region where all crown ether voids are saturated with Rb^+ or K^+, as mentioned in detail in the explanation of the absorbance change

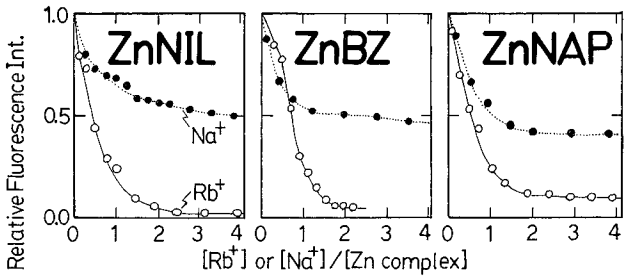

Figure 11. Intensity decrease of S_1 emission of Zn complexes upon addition of Na^+ (●) or Rb^+ (○) in $CHCl_3$. The intensity in the absence of cation was set at unity.

upon cation addition (Figure 3). Accordingly, in the latter region, rigid eclipsed dimers are present and a weak, constant residual fluorescence is due to the small amount of monomer species in equilibrium with the cofacial species, indicating that cofacial species do not emit or emit very weakly, if any.[34]

The effect of Na^+ is of course less than Rb^+, but it is still effective. Quenching occurs efficiently in the $0 < [Na^+]/[\text{ligand}] < 1$ region, and above $[Na^+]/[\text{ligand}]$ = *ca.* 1.5 or 2 the intensity becomes almost constant. The residual intensity has an excitation spectrum identical with that of monomer species and therefore is perhaps attributable to some amount of monomer species in equiliblium with cofacial dimers. The larger residual intensity in Na^+ added systems compared to Rb^+ systems would imply that monomers are more abundant in the former systems. Although not shown, the residual intensity changes only slightly in the $2 < [Rb^+]$ or $[Na^+]/[\text{ligand}] < 20$ region, indicating that further oligomerization does not occur in this region. Also, it is interesting to note that the relative residual fluorescence intensity at a fixed $[Na^+]/[\text{Zn complex}]$ becomes smaller with increasing area of the π-systems. For example, at $[Na^+]/[\text{Zn complex}]$ = *ca.* 2, the values are 0.57, 0.50, and 0.42 for ZnNIL, ZnBZ and ZnNAP, respectively.

(vi) Time-Resolved EPR (TREPR) Spectra. TREPR spectra could be observed for all the zinc complexes and typical examples are shown in Figure 12. These spectra come from polarized excited triplet (T_1) states produced by anisotropic intersystem crossing (isc) (P_i; $i = x, y, z$) from S_1. The polarization pattern of *A*/*E*, *A* at lower stationary fields (*h*/*x*, *y*, *z*) and *E* at higher stationary fields (*A* and *E* denote absorption and emission of microwaves, respectively), is the same as those of other zinc Pc and porphyrin (Por) complexes.[1m,35] The spectra were simulated with P_i's and zero field splitting (zfs) parameters, *D* and *E*, under consideration of random orientations of molecules in glass. The simulated spectra ($g = 2.0$) and the obtained values are shown in Figure 12 and Table 5. It was found that both a monomer and the dimer contributed to the observed spectra of ZnNIL and ZnNAP, but the dimer spectrum was clearly separated from the monomer one for ZnBZ. The *D* value ($= -3z/2$; *z* is the direction toward an out of Pc plane) of the monomer becomes smaller in the order of ZnNIL, ZnBZ, and ZnNAP. For the *E* value ($= |x - y|/2$; a measure of anisotropy within the ring plane), a slightly larger value was obtained for ZnBZ. On dimerization, remarkable decrease in *D* was observed.

The zfs parameter *D* reflects anisotropic distribution of unpaired electrons towards an out of plane axis, *z*, with respect to that in the ring plane (*x*, *y*). Therefore the decreases in *D* are qualitatively interpreted by delocalization of the unpaired

(31) Kobayashi, N.; Ashida, T.; Hiroya, K.; Osa, T. *Chem. Lett.* **1992**, 1567: Kobayashi, N.; Ashida, T.; Osa, T. *Chem. Lett.* **1992**, 2031. Kobayashi, N.; Ashida, T.; Osa, T.; Konami, H. *Inorg. Chem.* **1994**, *33*, 1735.

(32) Muralidharan, S.; Ferraudi, G.; Patterson, L. K. *Inorg. Chim. Acta* **1982**, *65*, L235.

(33) Generally, subnanosecond lifetimes have been reported for the fluorescence of Pcs: Menzel, E. R.; Rieckhoff, K. E.; Voigt, E. M. *Chem. Phys. Lett.* **1972**, *13*, 604. Brannon, J. H.; Magde, D. *J. Am. Chem. Soc.* **1980**, *102*, 62.

(34) In the porphyrin system, cofacial dimer units emit more weakly than monomer: Kagan, N. E.; Mauzerall, D.; Merrifield, R. B. *J. Am. Chem. Soc.* **1977**, *99*, 5486. Chang, C. K.; Kuo, M.-S.; Wang, C.-B. *J. Heterocycl. Chem.* **1977**, *14*, 943. Chang, C. K. *J. Heterocycl. Chem.* **1977**, *14*, 1285. Guckel, F.; Schweiser, D.; Collman, J. P.; Bencosme, S.; Evitt, E.; Sessler, J. *Chem. Phys.* **1984**, *86*, 161. Mialoco, C.; Giannotti, A.; Maillard, P.; Momenteau, M. *Chem. Phys. Lett.* **1984**, *112*, 87.

(35) (a) Ishii, K.; Yamauchi, S.; Ohba, Y.; Iwaizumi, M.; Hirota, N.; Maruyama, K.; Osuka, A. *J. Phys. Chem.* **1994**, *98*, 9431. (b) Akiyama, K.; Tero-Kubota, S.; Ikegami, Y. *Chem. Phys. Lett.* **1991**, *185*, 65. (c) van Dorp, W. G.; Schoemaker, W. H.; Soma, M.; van der Waals, J. H. *Mol. Phys.* **1975**, *30*, 1701.

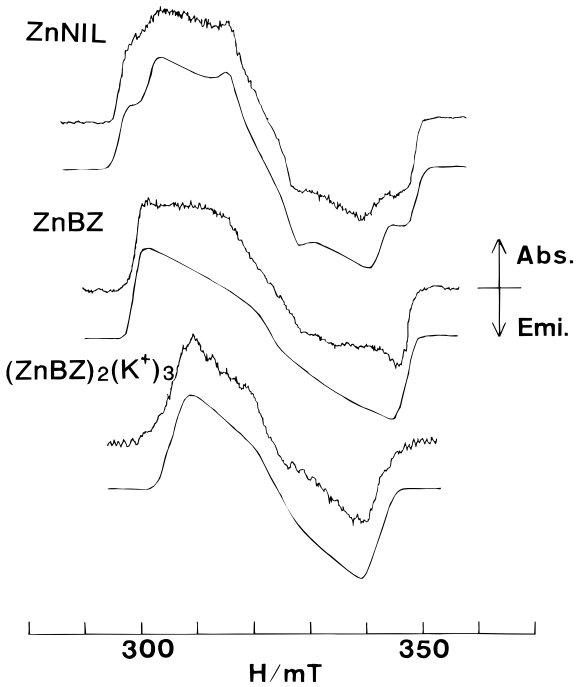

Figure 12. Time-resolved EPR spectra of ZnNIL (top), ZnBZ (middle), and $[ZnBZ]_2(K^+)_3$ (bottom) observed at 77 K in EtOH−$CHCl_3$ (1:1 v/v) with their simulations. The spectra were taken at 0.5 μs after laser excitation at 640 nm.

Table 5. Zfs Parameters Obtained from the Simulation

compd	*D*/GHz	*E*/GHz	P_x:P_y:P_z
ZnNIL	0.743	0.138	0:0.l:0.9
ZnBZ	0.698	0.208	0:0.3:0.7
(ZnBZ)2	0.555	0.135	0:0.3:0.7
ZnNAP	0.690	0.130	0:0.15:0.85

Table 6. Calculated Zfs Using a Half Point Charge Approximation

compd	*D*/GHz	*E*/GHz
ZnNIL	0.609	0.131
ZnBZ	0.605	0.125
ZnNAP	0.563	0.126

π-electrons over additionally fused benzo and naphtho rings in the monomers and over another monomer unit in the dimer. In order to check these changes more quantitatively, we have first calculated the zfs of T_1 monomer by using HOMO and LUMO of Pc analogues under a half point charge approximation.[36,37] The results were summarized in Table 6. It is found that the amounts of the changes in the *D* values are consistent with our consideration. The larger *E* value observed for ZnBZ may be interpreted in terms of a pseudo-Jahn−Teller distortion,[38] because the LUMO and the next LUMO are considered to be close in energy for ZnBZ.[36]

For the dimer, we have already proposed a novel method for qualitative analysis by using the *D* value as the following: on the bases of the valence bond (VB) method any wave function of the T_1 dimer (DM) is described by a linear combination of two types of excited states as

$$^3\Phi_{DM} = a^3\Phi_{EX} + b^3\Phi_{CR} \quad (2)$$

Here EX (exciton) and CR (charge resonance) denote an excitation localized and delocalized type, respectively. Superscript 3 means the excited triplet state. For the sandwich type parallel dimer as $D_{EX} = D_M$ (M; monomer),[1m,35a,39] an extent of excitation delocalization over both rings, b^2, is obtained from the equations

$$D_{DM} = a^2D_{EX} + b^2D_{CR} \quad (3)$$

$$b^2 = (D_M - D_{DM})/(D_M - D_{CR}) \quad (4)$$

Using the observed *D* values of the monomer ($D_M = 0.698$ GHz) and the dimer ($D_{DM} = 0.555$ GHz) and the calculated *D* value for the CR state ($D_{CR} = -0.182$ GHz) under a point charge approximation,[1m,35a,39] b^2 was obtained as 0.16. This value is very similar to that reported for a crown-ether bridged zinc porphyrin (0.16)[1m] and is larger than those obtained for several kinds of aromatic ring-bridged zinc porphyrins.[35a] This indicates that the crown-ether bridges play an apparent role for an interplanar interaction in the dimer.

The predominant isc to T_z ($P_z \gg P_x$, P_y) is interpreted by participation of the d orbitals (d_{xz}, d_{yz}) of the Zn atom in the $T_1(\pi-\pi^*)$ state,[35c] which presents striking contrast to those for metal-free Pc and MgPc (P_x, $P_y \gg P_z$).[1m,35b]

(vii) Molecular Orbital (MO) Calculations. The spectra of metallophthalocyanines with D_{4h} symmetry have most widely been described by Gouterman's four-orbital model[40] in which the optical spectrum can be interpreted in terms of a_{1u} highest occupied molecular orbital (HOMO), the a_{2u} second HOMO, and the doubly degenerate e_g lowest unoccupied molecular orbitals (LUMOs). Unlike the situation with porphyrins, the aza nitrogens at the meso positions and fused benzenes separate the a_{1u} and a_{2u} orbitals to dramatically increase the requirement for intensity mixing between the lowest two singlet excited states, Q and B1, so that the intense Q and B1 bands generally appear at around 660−700 and 320−360 nm.[41,42] The next band called the B2 band[24a] appears *ca.* 2000−7000 cm^{-1} above the B1 band, while the next higher band called the N band with lower intensity appears at around 250−300 nm. This feature is shown in Figure 13. Although the Q band is relatively pure, other bands are mixtures of several configurations, and can not be described by a one-electron description. Therefore, the transitions shown in this figure represent a first-order assignment.[24a,40]

With the lowering of molecular symmetry to C_{2v}, the e_g orbitals split into two nondegenerate b_1 and b_2 orbitals. As shown in Figure 13, transitions from the $a_1(\pm4)$, $a_2(\pm4)$, $a_1(\pm2)$, and another $a_1(\pm2)$ orbitals to $b_1(\pm5)$ and $b_2(\pm5)$ orbitals become allowed in this symmetry (angular momenta in parentheses). In order to correlate the transitions in Figure 13 and to enhance our interpretation of the electronic absorption (and MCD) spectra of monomer species, MO calculations have been performed for the (pyrrole proton) deprotonated dianionic species (*i.e.*, NIL^{2-}, BZ^{2-}, NAP^{2-},and, in addition ANT^{2-}, the dianion of monoanthracotribenzoporphyrin) within the frame-

(36) LCAO coefficients obtained in the MO calculations in the following section (section vii) were used.

(37) Yamauchi, S.; Hirota, N.; Higuchi, J. *J. Phys. Chem.* **1988**, *92*, 2129.

(38) Chan, I. Y.; van Dorp, W. G.; Schaafsma, T. J.; van der Waals, J. H. *Mol. Phys.* **1971**, *22*, 741.

(39) Yamauchi, S.; Konami, H.; Hatano, M.; Ohba, Y.; Iwaizumi, M. *Mol. Phys.* **1994**, *83*, 335.

(40) Gouterman, M. In *The Porphyrins*; Dolphin, D., Ed.; Academic Press: New York, 1978; Vol. III, Part A, pp 1−165. Gouterman, M. *J. Chem. Phys.* **1959**, *30*, 1139.

(41) Schaffer, A. M.; Gouterman, M.; Davidson, E. R. *Theor. Chim. Acta* **1973**, *30*, 9.

(42) McHugh, A. J.; Gouterman, M.; Weiss, C. *Theor. Chim. Acta* **1972**, *24*, 346. Dedieu, A.; Rohmer, M. M.; Veillard, A. *Adv. Quantum. Chem.* **1982**, *16*, 43. Orti, E.; Bredas, J. L.; Clarisse, C. *J. Chem. Phys.* **1990**, *92*, 1228. Rosa, A.; Baerends, E. J. *Inorg. Chem.* **1992**, *31*, 4717. Ishikawa, N.; Ohno, O.; Kaizu, Y. *J. Phys. Chem.* **1993**, *97*, 1004. Henrikson, A.; Roos, B.; Sundobom, M. *Theor. Chim. Acta* **1972**, *27*, 303.

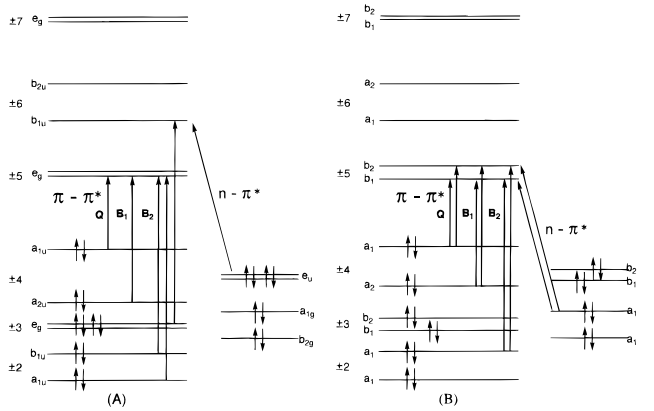

Figure 13. (A) Frontier molecular orbitals in D_{4h} symmetry involved in the major $\pi-\pi^*$ absorption transitions with energies lower than *ca.* 38 000 cm^{-1}. The order of the orbital is based on theoretical models for ZnPc(−2) species[24a,25] and the results in the present calculations. The Q, B1, and B2 transitions shown are those anticipated through application of Gouterman's four-orbital LCAO model[40] and from analysis of MCD data of Zn- and MgPc.[24a,25] The arrows indicate allowed transitions that give rise to bands observed in the 300−800 nm region of the absorption and MCD spectra. Each of the state generated will be degenerate, and MCD *A*-terms are observed for each transition. Numbers with ± indicate orbital angular momenta. (B) Frontier molecular orbitals in C_{2v} symmetry involved in the major $\pi-\pi^*$ transitions with energies lower than *ca.* 38 000 cm^{-1} adapted from Schaffer *et al.*[41] No account has been taken of changes in the energies of the molecular orbitals as a result of different symmetry from (A). The possible $\Delta M_L = \pm 1$ transitions are shown based on application of Gouterman's four-orbital LCAO model[40] as shown for (A). The orbitals shown are labeled for the C_{2v} symmetry and were obtained from the corresponding D_{4h} labeling through the use of correlation tables.

work of the PPP approximation. Parameters are the same as those introduced in a previous publication,[30] which have been proven to be reliable. For example, for Pc^{2-}, the calculations reveal the Q and Soret transitions to be at 662 and 332 nm, which are in good agreement with previously reported experimental data.[24] In the cases of NIL^{2-} and NAP^{2-} with C_{2v} symmetry, the degenerate pairs of orbitals comprising the lowest and fourth lowest unoccupied and the third highest occupied levels in BZ^{2-} (*i.e.*, D_{4h} symmetry, Figure 13(A)) split into two levels each, and therefore it is anticipated that the spectra become more complex. However, as shown below, the MO calculations have succeeded in reproducing the spectroscopic characteristics mentioned in (iv), and further gave information which appear useful in interpreting the experimental spectra. The main results of the calculations are summarized as follows (see also Table 7). (i) The Q band split into two (as shown typically in Figure 7), but the splitting in NIL^{2-} (526 cm^{-1}) is larger than NAP^{2-} (237 cm^{-1}). In ZnNIL and ZnNAP, the values are 1423 and 282 cm^{-1}, respectively, and in CuNIL and CuNAP these are 808 and 340 cm^{-1}, respectively. This is consistent with the previously accummulated fact that the substituent effect is larger the smaller the size of the parent molecules.[24b] (ii) As judged from the comparison of oscillator strengths in Table 7, of the two split bands, the band to lower energy ($a_1(\pm4) \rightarrow b_1(\pm5)$) is stronger for NIL^{2-} but weaker for NAP^{2-}. This inversion occurs at BZ^{2-}, because the intensity of the degenerate two Q bands of BZ^{2-} is the same (see Table 7). In order to confirm this tendency, we calculated also the MOs of the monoanthraco analogue, *i.e.*, ANT^{2-}, and the results are included in Table 7. As seen, the relative strength of the second Q band ($a_1(\pm4) \rightarrow b_2(\pm5)$) to the first Q band increases in the order NIL^{2-} (0.90), BZ^{2-} (1.00), NAP^{2-} (1.10), and ANT^{2-} (1.23), *i.e.*, with the increase of molecular size of fused aromatics. Such a tendency has not been reported to date,

Table 7. Calculated Transition Energies, Oscillator Strengths (*f*), and Configurations for Deprotonated Pc Derivatives[a]

energy/eV(nm)	*f*	configurations[b]		
		NIL^{2-}		
1.92892 (643)	0.70	19→20(87%)	18→21(13%)	
1.99413 (622)	0.63	19→21(84%)	18→20(16%)	
3.51648 (353)	1.10	18→20(30%)	17→20(27%)	16→20(27%)
3.70328 (335)	1.34	18→20(38%)	16→20(35%)	17→20(11%)
3.80931 (325)	2.11	18→21(63%)	13→21(12%)	19→20(11%)
3.99365 (310)	0.30	12→20(67%)	19→23(16%)	
4.15704 (298)	0.16	15→20(40%)	13→21(29%)	16→21(22%)
4.46007 (278)	0.17	19→25(45%)	17→21(15%)	16→21(12%)
		BZ^{2-}		
1.87357 (662)	0.84	21→22(87%)	20→23(12%)	
1.87357 (662)	0.84	21→23(87%)	20→22(12%)	
3.73470 (332)	2.19	20→23(67%)	13→23(12%)	21→22(11%)
3.73470 (332)	2.19	20→22(67%)	13→22(12%)	21→23(11%)
4.11100 (302)	0.25	16→22(23%)	21→27(20%)	13→22(15%)
			16→23(14%)	21→26(12%)
4.11100 (302)	0.25	16→23(23%)	21→26(20%)	13→23(15%)
			16→22(14%)	21→27(12%)
4.24330 (292)	0.27	21→27(64%)	16→22(13%)	
4.24330 (292)	0.27	21→26(64%)	16→23(13%)	
		NAP^{2-}		
1.81979 (681)	0.90	23→24(89%)	21→25(11%)	
1.84198 (673)	0.99	23→25(88%)	21→24(11%)	
3.52917 (351)	1.72	22→25(46%)	21→24(38%)	
3.76872 (329)	2.06	21→25(71%)		
3.85608 (322)	0.54	22→25(43%)	21→24(28%)	
4.19372 (296)	0.21	23→29(36%)	20→24(24%)	15→24(14%)
4.23624 (293)	0.15	20→24(66%)		
4.71329 (263)	0.61	22→26(57%)	15→25(18%)	14→24(16%)
		ANT^{2-}		
1.78867 (693)	0.90	25→26(89%)		
1.83323 (676)	1.11	25→27(89%)		
3.23727 (383)	0.58	24→27(63%)	25→29(16%)	
3.73149 (332)	2.10	23→26(60%)	24→27(11%)	
3.82358 (324)	2.21	23→27(43%)	25→30(17%)	24→28(12%)
3.85049 (322)	0.33	25→30(60%)	24→28(19%)	
4.06174 (305)	0.15	25→31(51%)	17→26(35%)	
4.14686 (299)	0.39	22→26(28%)	25→31(26%)	17→26(24%)
		19→28(12%)		
4.23818 (293)	0.15	25→33(36%)	20→27(27%)	21→26(20%)
4.64845 (267)	0.22	19→27(40%)	17→27(38%)	

[a] Excited states with less than 5.0 eV and *f* greater than 0.15 are shown. [b] Orbital numbers 19, 21, 23, and 25 are HOMOs of NIL^{2-}, BZ^{2-}, NAP^{2-}, and ANT^{2-}, respectively. In NAP^{2-}, the MOs numbered 22 (the second HOMO) and 26 (the third LUMO) are naphthalene-centered orbitals. Similarly, in ANT^{2-}, the second HOMO (MO number 24) and the third LUMO (MO number 28) are anthracene-centered orbitals. These naphthalene and anthracene-centered orbitals are not included in the energy diagram of Figure 13B.

although, of the split Q bands of other tribenzotetraazaporphyrins, the band to the longer wavelength ($a_1(\pm4) \rightarrow b_1(\pm5)$) is always stronger, consistent with the above results.[22a] (iii) The Q band energy, defined as the mid-energy between the split Q bands, shifts to longer wavelength in the order NIL^{2-}, (632 nm), BZ^{2-} (662 nm), and NAP^{2-} (676 nm), in accord with the experimental order. For example, experimental values for zinc complexes are 661, 683, and 705 nm for ZnNIL, ZnBZ, and ZnNAP, respectively (values for ZnBZ and ZnNAP are the average values of a Q MCD peak and trough, *i.e.*, two *B* terms of opposite sign). (iv) In a one-electron description, the Q band to lower energy corresponds to a transition from the HOMO to the LUMO ($a_1(\pm4) \rightarrow b_1(\pm5)$), while that to higher energy corresponds to one from the HOMO to the second LUMO ($a_1(\pm4) \rightarrow b_2(\pm5)$), also in accordance with Figure 13. Thus, for example, in ZnNIL the bands at 686 and 625 nm, respectively, correspond to the above transitions. However, their

"purity" increases with increasing molecular size as suggested from their configuration. Taking the instance of the Q band to the higher energy, the percentage of the HOMO to the second LUMO transition increases from 84% of NIL^{2-} to 87% of BZ^{2-} and further to 88% of NAP^{2-} and 89% of ANT^{2-}. The situation in the Q band to the lower energy is the same. (v) The features in the shorter wavelengths are very complex. The split B1 bands are no longer described in a one-electron description, since they appear to be mixtures of several configurations. For NIL^{2-}, two bands are estimated to lie at 353 and 335 nm, and transitions to the LUMO from the second, third, and fourth HOMOs appear to contribute comparably. Interestingly, contribution of a transition from the second HOMO to the second LUMO (orbital number 18 to 21) is not included in this band, although this band is allowed (Figure 13(B)). For NAP^{2-}, two bands are calculated at 351 and 329 nm. For the 351 nm band, transitions from the second HOMO to the second LUMO and the third HOMO to the LUMO are the main contributions (note that the second HOMO (MO number 22) and the third LUOMO (MO number 26) are naphthalene-centered MOs). The 329 nm band corresponds to one of the split B1 components and relatively pure and strong. Judging from the similarity of configurations, the bands at 351 and 322 nm may constitute one set, plausibly the split two components of either B1 or B2 band. In 260−360 nm of the spectra of NIL^{2-} and NAP^{2-}, six transitions are recognized when f greater than 0.15 are listed (Table 7). (vi) The lower energy shift of the Q band on going from MtNIL, MtBZ, and MtNAP (Mt = Zn or Cu) may be largely explained as a destabilization of the HOMOs on ring expansion, since the first HOMOs in NIL^{2-}, BZ^{2-}, and NAP^{2-} are predicted at −7.7496, −7.4869, and −7.3728 eV, respectively, while the energy of the first LUMOs in these systems are close to one another (−3.9378, −3.7442, and −3.7447 eV, respectively).

Concluding Remarks

Monomers and cation-induced dimers of low symmetrical Pc analogues substituted with three crown ether voids have been analyzed by various spectroscopies including electronic absorption, magnetic circular dichroism, fluorescence emission, NMR, EPR, and time-resolved EPR. Electronic absorption spectra of monomers have been reproduced by molecular orbital calculations within the framework of the approximation treating only π-electrons. From the change of absorption and emission spectra, it was found that the dimerization is a two-step three-stage process, and the final stage cofacial dimers are eclipsed C_{2v} type with a center−center separation of 4.1−4.2 Å without depending on the diameters of the cations used. Analysis of time-resolved EPR spectra showed delocalization of excited π-electrons over monomer chromophores and two macrocycles in the dimers. The monomers showed both S_1 and S_2 emissions whose quantum yields and lifetimes are smaller than those of the corresponding symmetrical D_{4h} species.

Acknowledgment. We thank Dr. H. Konami for his help in MO calculations.

JA950929X